9. The Carbon Cycle and Climate

9.1. Role of carbon in the earth system

The element carbon is central to our studies of the greenhouse effect and climate change, through the infrared emission and absorption processes of atmospheric CO_2 and CH_4 (Chapter 2). It is a measure of the health of our land and ocean biosphere in terms of standing biomass and NPP (Chapter 8). It is also intimately linked to our energy supplied from fossil fuels (Chapter 11). The role of precipitating marine organisms in transporting carbon from the upper ocean into sediments, described as the "biological pump", is crucial in understanding the carbon cycle on geological time scales, as well for an annual budget, and future climate change. It may be surprising that making cement from sediments is an important source of CO_2, which is given off when calcium carbonate ($CaCO_3$) in limestone is heated in a kiln. The role of land vegetation in the annual budget and future climate change is also critical, with key issues including afforestation versus deforestation and the role of high latitude soils in a warming climate.

On geological time scales, there is ~10,000 times as much carbon stored in the crust and mantle compared to that stored in the ocean, atmosphere, and biosphere. Changes in the amount of carbon stored in the crust and mantle are likely to be responsible for the warm and cold periods observed at 100 million-year time scales (Robert Hazen, Suarez et al. 2019). In the past 500 million years, there have been four periods of enhanced volcanic emissions, lasting about 10,000 yr, which roughly doubled atmospheric CO_2 amounts. Large bolide impacts such as the Chicxulub event in the Yucutan ~ 65 Mypb can also release large quantities of trapped carbon, which, after a few years of cooling by obscuring the sun, leads to a warmer climate through the greenhouse effect. It has been estimated that yearly anthropogenic carbon fluxes into the atmosphere currently exceed the fluxes associated with massive volcanic eruptions and bolide impacts. Frozen methane clathrates in ocean shelf sediments represent a possible fuel reservoir which exceeds known reserves of petroleum (section 9.5).

9.2. A global carbon budget from ~1990 and the missing carbon sink problem

The amount of carbon in a given reservoir is measured in terms of gigatons (Gt), where 1 Gt = 10^9 tons = 10^{12} kg = 10^{15} g = 1 Pg. Fluxes are given in Gt/yr, with a positive value corresponding to an increase in a given reservoir (a source). The net flux into a reservoir is given by the sources minus the sinks. If the net flux is not zero, this implies a trend in the reservoir. If the trend estimated from using a box model disagrees with the observed trend, this is an indication that there are uncertainties in some of the calculations.

A useful concept is the *residence time* (in years) for a reservoir, which is defined as the reservoir amount in Gt divided by the sum of the sinks for that reservoir (in Gt/yr).

One may convert between ppmv CO_2 and Gt carbon as follows: 1 ppmv CO_2 x (12 kg C / 44 kg CO_2) x (44 kg CO_2 / 29 kg air) x (5×10^{18} kg air) ~ 2 Gt. Therefore, a rate of increase of 1 ppmv/yr CO_2 equals an increase of 2 Gt C/yr in the atmosphere, which is about 0.3%/yr.

Figure 9.1 shows a box model with reservoir and flux estimates from ~1990. In increasing order, the reservoir amounts shown are: atmosphere 740 Gt, land biosphere 2,100 Gt, fossil fuels 7,500 Gt, the ocean 38,000 Gt, and sediments 20,000,000 Gt. By the early 1990s, the land biosphere was estimated to absorb and emit 120 Gt/yr through photosynthesis and respiration, with 2 Gt/yr extra estimated due to deforestation. The ocean was estimated to absorb 107 Gt/yr through photosynthesis and emit 105 Gt/yr through respiration, showing a net sink to the atmosphere of 2 Gt/yr, due to the "biological pump". Fossil fuel burning was estimated to emit 5 Gt/yr to the atmosphere, with cement making added another 1 Gt/yr. The net effect of the "biological pump" (-2 Gt/yr) approximately offset the effects of deforestation (+2 Gt/yr), yielding an estimated net flux into the atmosphere from fossil fuel burning and cement making of 6 Gt/yr.

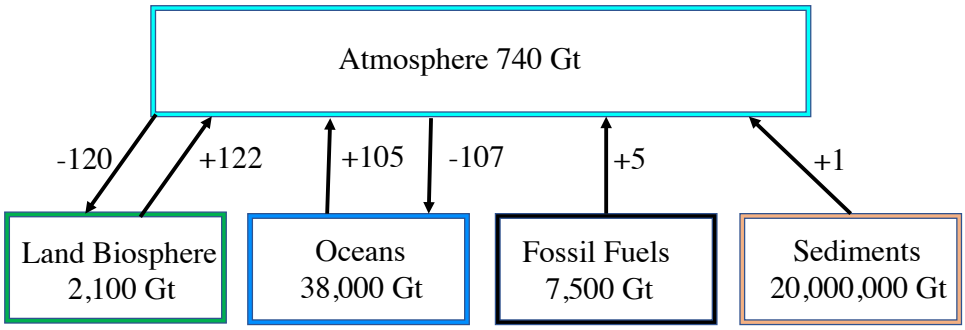

Figure 9.1. Global carbon reservoirs in Gt with fluxes in Gt/yr estimated circa 1990. The land biosphere was estimated to absorb and emit 120 Gt/yr through photosynthesis and respiration, with a net source to the atmosphere of 2 Gt/yr extra due to deforestation. The ocean was estimated to absorb 107 Gt/yr due to photosynthesis and emit 105 Gt/yr due to respiration, with a net sink to the atmosphere of 2 Gt/yr, due to the "biological pump". Fossil fuel burning was estimated to be emitting 5 Gt/yr, with cement making added another 1 Gt/yr.

However, the observed trend in the atmospheric carbon reservoir in the early 1990s was ~1.5 ppmv/yr ~ 0.4%/yr ~ 3 Gt/yr, compared to the net flux estimate from the geophysical box model of 6 Gt/yr. This discrepancy of order 50% became known as the "missing carbon sink problem". Since the rate of usage of fossil fuels and cement are based on comparatively accurate business records, this helped motivate funding of more detailed observational and analytical studies of carbon fluxes between the atmosphere and ocean, and between the atmosphere and the land biosphere. A fundamental challenge in solving the "missing carbon sink problem" is that variation in carbon fluxes occur on the spatial and time scale of the variation in vegetation and ocean eddies. In addition, natural climate variations, such as ENSO, cause interannual variability in carbon fluxes of order +/- 2 Gt/yr.

It is of interest to consider the residence time of carbon in the atmosphere, land biosphere, and ocean. From Fig. 9.1, the sum of the sinks to the ocean and land from the atmosphere due to photosynthesis is 227 Gt/yr. With an atmospheric reservoir of 740 Gt, this

implies a residence time of ~ 3 years for atmospheric CO_2 against photosynthesis. This is much smaller than the residence time of ~90 years for CO_2, considering only loss by photolysis by ultraviolet, which only occurs at very high altitudes. It is the result of a strong biosphere. One may observe that, as the atmospheric reservoir carbon increases, and if oceanic uptake diminishes, that the lifetime of carbon in the atmosphere will increase.

The land biosphere contains 2100 Gt of carbon. With a respiration rate of 122 Gt/yr, the lifetime of carbon in the land biosphere is ~20 years. But the same estimation for the ocean, with 38,000 Gt carbon and a sink rate of 105 Gt/yr, gives a lifetime for oceanic carbon of ~380 years! This implies that if we stop burning fossil fuels today, the overburden in the atmosphere will go into the ocean, but then there will be an extra amount in the ocean that will then be returned to the atmosphere, by Henry's Law, and this will take several hundred years. That is, what we have put into the ocean will provide a protracted period of elevated atmospheric CO_2 for a long time. If we assume that atmospheric CO_2 doubles by the year 2100, and then we stop burning fossil fuels, until that time there will be a net flux of CO_2 into the oceans from the overburdened atmosphere. So, the oceans will "buffer" the atmosphere, delaying a reduction in atmospheric CO_2 for several centuries.

The estimated emission of carbon to the atmosphere by fossil fuel burning during 1850-1993 is shown in Fig. 9.2., with rapid growth occurring from ~1 Gt/yr in 1950 to ~6 Gt/yr in 1993.

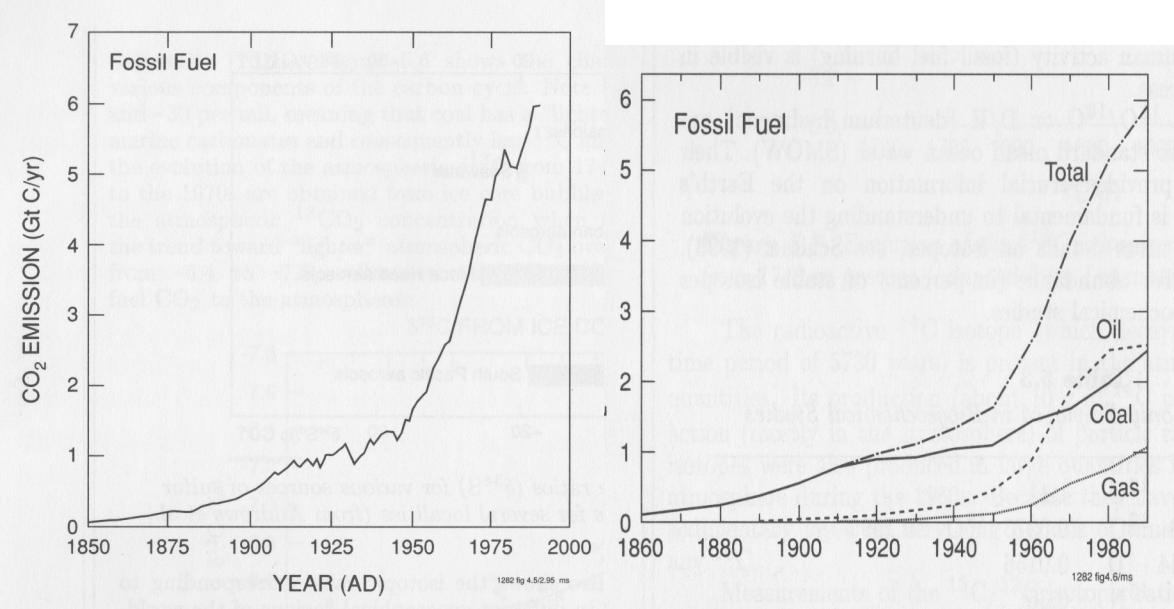

Figure 9.2. Estimated emissions of carbon to the atmosphere in Gt/yr resulting from fossil fuel burning during 1850-1993, with relative contributions by coal, oil, and natural gas shown at right (Figs. 5.9 and 5.10 of Brasseur et al. 1999).

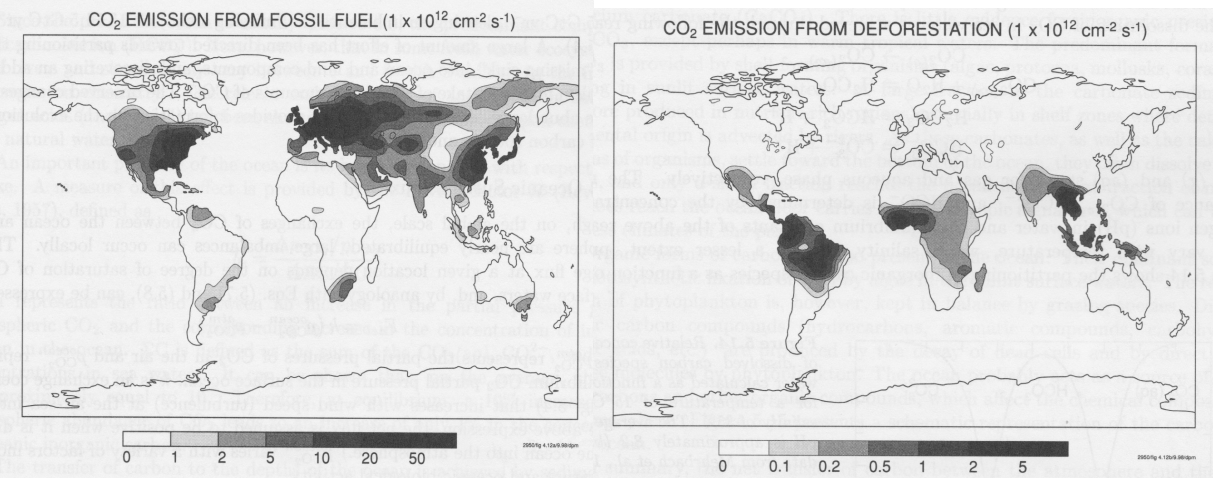

Figure 9.3. Distribution of emissions of carbon from (left) fossil fuels and (right) deforestation in 10^{12} cm^{-2} s^{-1} (Fig. 5.13 of Brasseur et al. 1999). Note that the shading scale is 10 times larger at left.

The geographical distribution of carbon fluxes into the atmosphere from fossil fuels and from deforestation are compared in Fig. 9.3. Fossil fuel emissions are highly correlated with the distribution of population, wealth, and industry, while fluxes into the atmosphere associated with deforestation are predominantly in tropical rainforests. Flux magnitudes are about 10 times larger from fossil fuel burning compared to deforestation. This clearly shows that anthropogenic greenhouse warming is largely driven by the economically developed nations.

Table 9.1 shows that tropical forests contain the most carbon, in phytomass above the soil, with temperate forests, boreal forests, and savanna also strongly contributing. However, a larger portion of the biomass exists in the soil, especially in the savanna, grassland, and wetlands ecosystems. This highlights the complexity of estimating carbon fluxes across ecosystems, and the different responses that each ecosystem might have to global warming.

Ecosystem Type	*Surface* (10^{12} m^2)	*NPP* (GtC yr^{-1})	*Phytomass* (GtC)	*Soils* (GtC)
Seasonal tropical forest	10.3	10.5	193	82
Evergreen tropical forest	4.5	3.2	51	41
Temperate forest	7.0	4.6	88	72
Boreal forest	9.5	3.6	96	135
Savanna	27.0	19.9	90	236
Grassland	12.5	4.4	9	295
Tundra	9.5	0.9	6	121
Semi-desert	21.0	1.3	7	168
Desert	24.5	0.1	1	23
Cultivated	16.0	6.8	3	128
Wetlands	3.5	4.0	15	225
Other	4.0	0.6	1	10
Total	149.3	59.9	560	1536

After Ajtay et al., 1979.

Table 9.1. Surface area, NPP, and carbon contained in the phytomass and in the soils for each ecosystem (Table 5.5 from Brasseur et al. 1999).

The average distribution of CO_2 fluxes between the atmosphere and ocean are shown in Fig. 9.4. In the tropics, the flux of CO_2 is generally from the ocean into the atmosphere, while in the high latitudes the flux is generally from the atmosphere to the ocean. Much of this can be attributed to Henry's Law, which describes the fact that, as a liquid is warmed, a greater portion of dissolved gas will enter the vapor state.

Dissolved CO_2 in warmer tropical waters tends to enter the vapor phase more easily, while CO_2 molecules striking the cold ocean surface at high latitudes tend to stick to the water. At high latitudes, annual phytoplankton blooms remove carbon from the upper ocean, making it easier for atmospheric CO_2 to enter the ocean. The likely effect of increasing global SSTs and of decreasing phytoplankton is to reduce the ability of the ocean to take up CO_2.

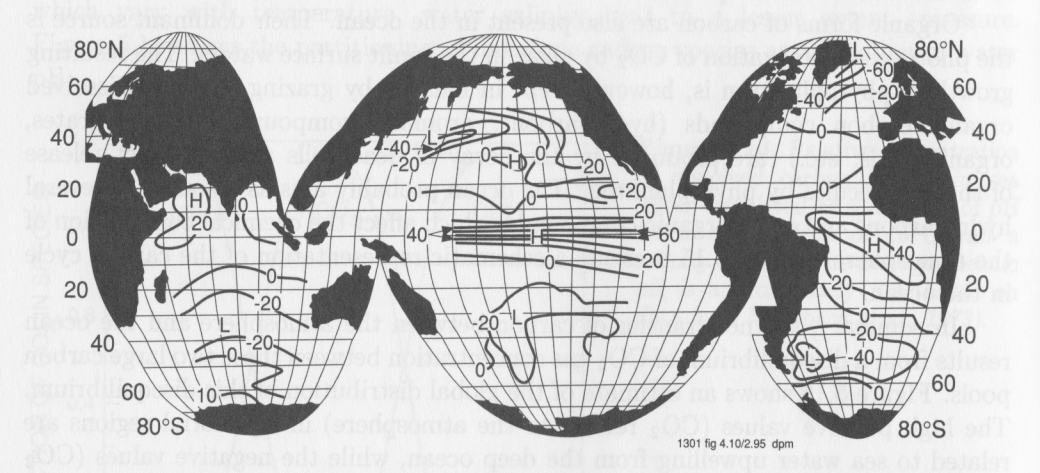

Figure 9.4. Difference in CO2 partial pressure (ppmv) between the ocean and the atmosphere, where a positive value implies a flux from the ocean into the atmosphere (Fig. 5.16 of Brasseur et al. 1999).

By the end of the 1990s, estimates of carbon sources due to tropical deforestation and sinks due to extratropical afforestation and ocean uptake had been revised, such that the difference of 4.6 Gt/yr between total known sources (7.1 Gt/yr) and the sum of known sinks (2.5 Gt/yr) was only 1.3 Gt/yr larger than the observed rate of increase (3.3 Gt/yr) (Table 5.4, Brasseur et al. 1999). By 2010 the missing carbon sink problem had largely been resolved through more detailed observations and analysis.

9.3. Carbon budget for 2016

Observed values of CO_2 at Mauna Loa (Fig. 9.5) show an increase from ~318 ppmv in 1958 to ~405 ppmv in 2016, which corresponds to an increase of ~27% or ~200 Gt C. The annual range due to the seasonal cycle of photosynthesis in the NH is ~10 ppmv.

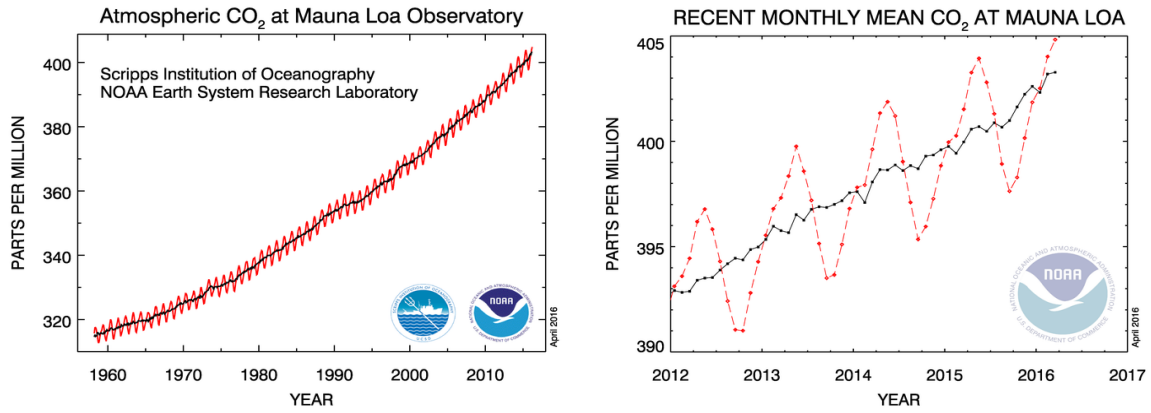

Figure 9.5. Observed values of CO_2 at Mauna Loa during 1958 – 2016 and monthly values during 2012-2016 (Global Carbon Project).

The annual growth rate of CO_2 at Mauna Loa is compared with fossil fuel emissions in Fig. 9.6. In the 1960s the growth rate was ~1 ppmv/yr (~2 Gt/yr), increasing to ~1.5 ppmv/yr (3 Gt/yr) in the 1990s, and by the 2000s it was ~2 ppmv/yr (~4 Gt/yr). Emissions of CO_2 grew from ~6 Gt/yr in the 1990s to ~10 Gt/yr by the end of the 2000s. An extrapolation to 2019 (right) suggests that we are currently probably emitting about 12 Gt/yr globally.

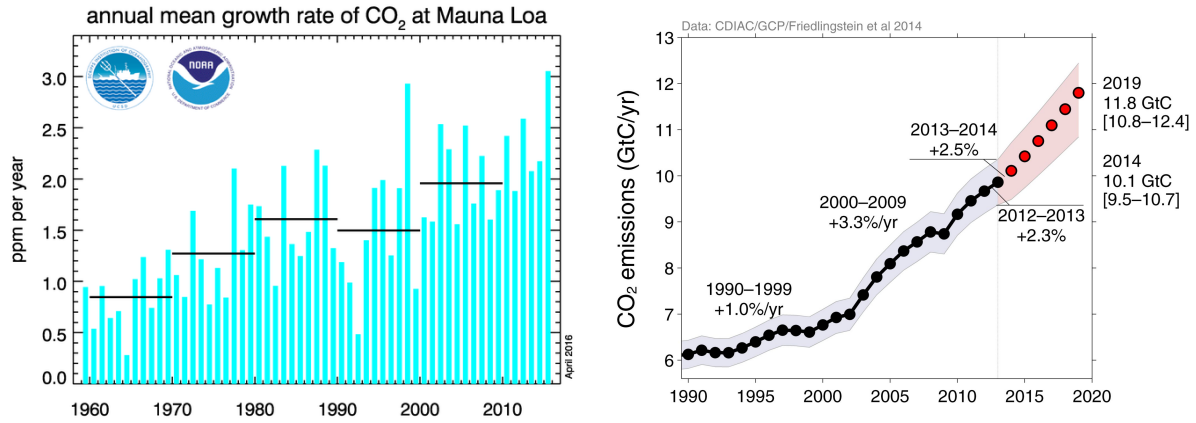

Figure 9.6. Annual mean growth rate of CO_2 (ppmv/yr) at Mauna Loa during 1958 – 2016 (left) and global CO_2 emissions (Gt/yr) during 1990 – 2014, with extrapolation from 2014 to 2019 (Global Carbon Project).

The economy and infrastructure of China has developed very rapidly during the past 20 years, with CO_2 emissions attributable to China increasing from ~1 to 3.5 Gt/yr (Fig. 9.7). During the past decade, there has been a noticeable increase in emissions from India, with a slight decrease in emissions from Europe. Emissions from the U.S.A. stayed roughly constant, with population increase being offset by increased efficiency, or reduced emissions per capita (Fig. 9.7, right). It should be noted that the rapid growth in coal consumption in China is related to the production of goods which are largely sold to Europe and North America.

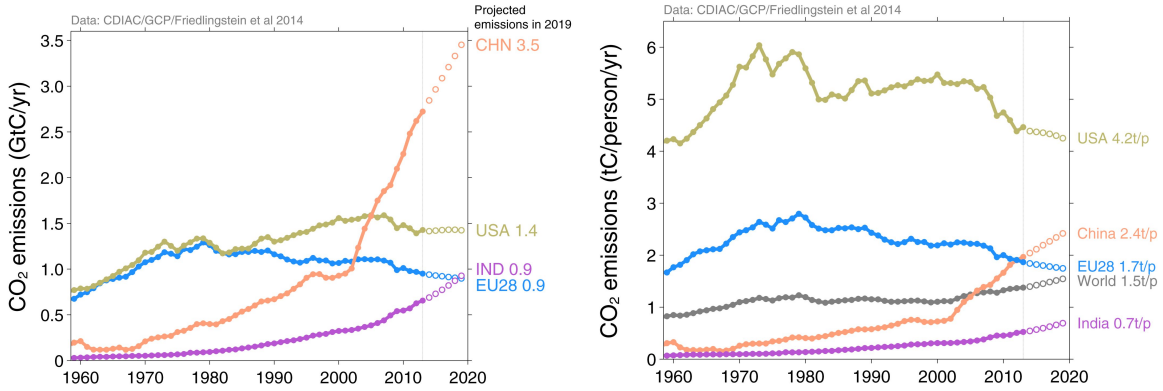

Figure 9.7. The history of estimated and extrapolated CO_2 emissions (Gt/yr) during 1960 – 2019 is shown together with that for CO_2 emissions per person (Global Carbon Project).

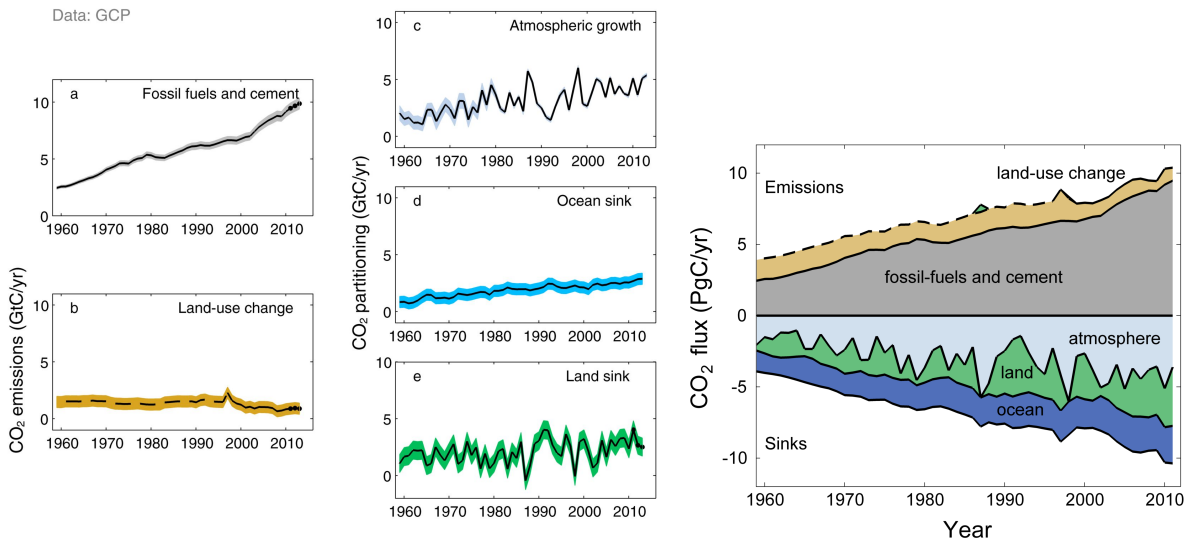

Figure 9.8. Evolution of carbon sources due to a) fossil fuels and cement, b) land-use change, c) observed atmospheric growth rate, and sinks due to d) the ocean, and e) the land biosphere during 1960-2012. The individual contributions in Gt/yr are shown together in the right panel (Global Carbon Project).

The evolution of sources, atmospheric storage, and sinks during 1960 – 2012 is shown in Fig. 9.8. The symmetry about the zero line in the right-hand panel reflects closure of the carbon budget by improved estimates for the land and ocean sinks. About 50% of the increase in fossil fuel input is being balanced by uptake in the ocean and land biosphere, with the other 50% going toward increases in atmospheric content.

Averaged over the past decade, CO_2 emissions of 9 Gt/yr have been balanced 46% by increases in the atmosphere (4.3 Gt/yr), 28% by increased uptake by the land biosphere (2.6 Gt/yr), and 26% by increased uptake by the ocean (2.5 Gt/yr). Strong interannual variability may be seen in the compensating changes in the rate of atmospheric increase and uptake by the land biosphere.

The partitioning of CO_2 emissions (Gt/yr) among cement making, gas, oil, and coal (left) during 1960-2014 is shown in Fig. 9.9. In 2000, emissions from coal burning began to exceed that from oil. In 2014, the relative contributions were: coal 43%, gas 34%, oil 18%, and cement 5%. The right-hand panel of Fig. 9.9 shows that economic crises are usually related to distinct periods of reduced emissions or rate of increase of emissions. This suggests that the health of the global biosphere is inversely proportional to conventional measures of economic productivity.

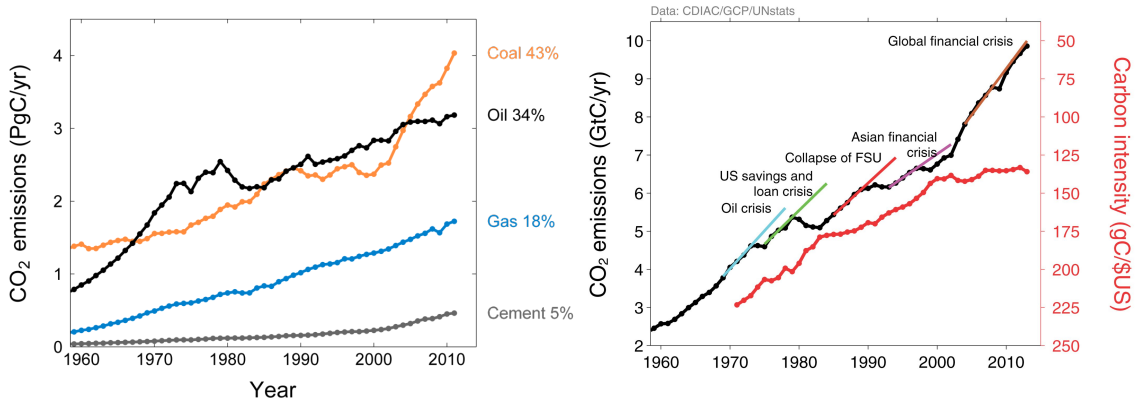

Figure 9.9. Partitioning of CO_2 emissions (Gt/yr) among cement making, gas, oil, and coal, together with changes of emissions related to significant economic events during 1960-2014 (Global Carbon Project).

9.4. Ocean acidification

The distribution of the column amount of carbon dissolved in the ocean which is attributable to increased CO_2 caused by humans is shown in Fig. 9.10. The two primary regions of subduction of surface waters are in the North Atlantic and in high latitudes of the SH. This increase in dissolved CO_2 has the effect of shifting the pH toward greater acidity.

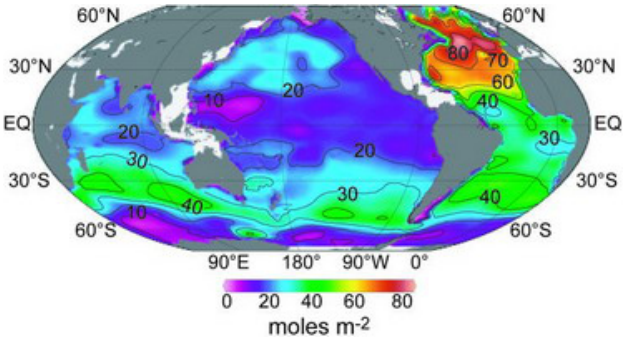

Figure 9.10. Distribution of column concentration of anthropogenic carbon dissolved in the oceans (moles m^{-2}).

The current distribution of the pH of ocean surface waters is shown in Fig. 9.11a. Most of the tropical and midlatitude waters have a pH of ~8.0-8.15, with somewhat higher values in the high latitudes and coastal regions. One estimate of the change in pH over the past 20 years is shown in Fig. 9.11b, with typical changes of -0.05 to -0.1. Note that the greatest acidification (orange) is occurring in the North Atlantic and circumpolar Antarctic oceans, where anthropogenic CO_2 is being subducted from surface waters into the deep ocean.

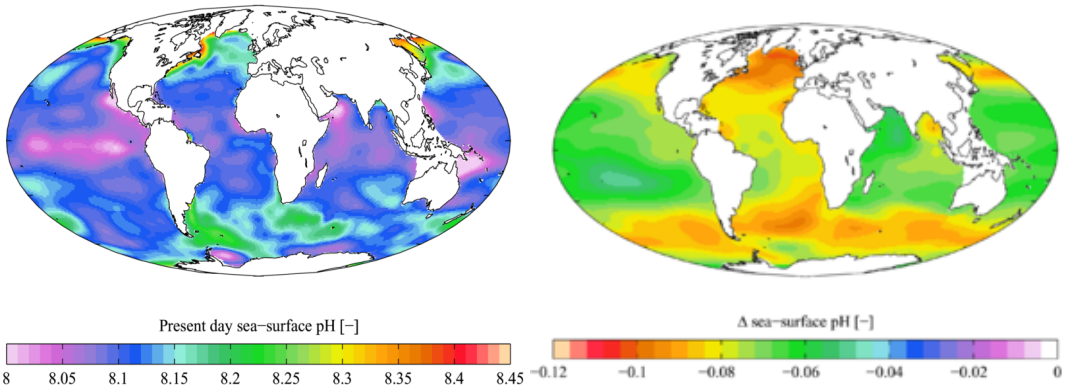

Figure 9.11. a) Distribution of pH at the sea surface and b) estimated change in pH over the past 20 years.

A recent study using the NCAR CCM3.1 (Fig. 9.12) shows the following changes. CO_2 in the atmosphere has increased from 278 ppm in pre-industrial times to ~420 ppmv today. During this time, the amount of CO_2 dissolved in the ocean has risen by more than 30%, decreasing the pH of the ocean by 0.11 units. As with CO_2 and global warming, there is some lag between cause and effect. That means that, even if all carbon emissions stopped today, we are committed to a further drop of up to 0.1 units.

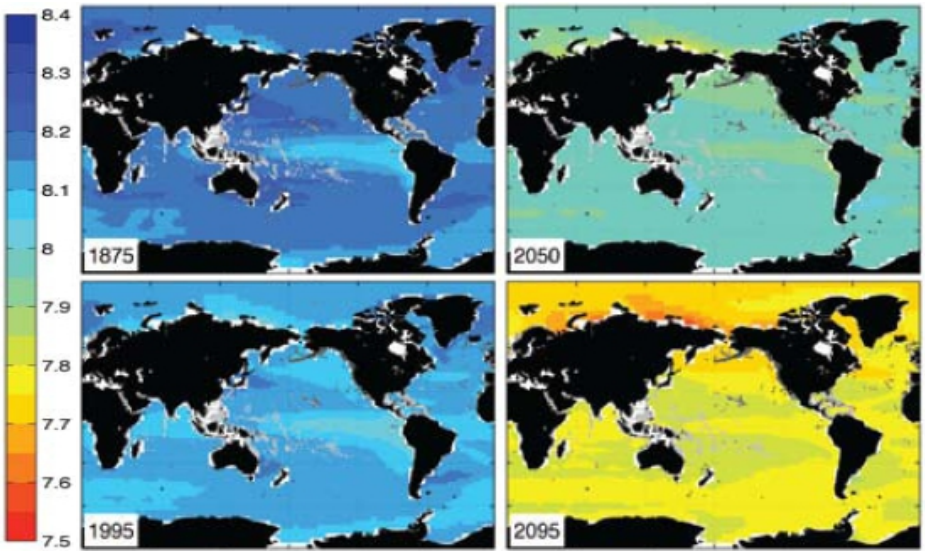

Figure 9.12. Distribution of pH at the sea surface for 1875, 1995, 2050, and 2095 A.D, estimated from the National Center for Atmospheric Research Community Climate Model 3.1.

The effect of increasing dissolved CO_2 is shown in Fig. 9.13. When carbon dioxide dissolves in water, it forms carbonic acid. The natural pH of rainwater is ~5.6 due to this effect. It also explains how carbonic acid can eat out limestone caves. In the oceans, carbonic acid releases hydrogen ions (H+), reducing pH, and bicarbonate ions ($HCO3^-$).

$$CO_2 + H_2O \rightarrow H^+ + HCO^-_3 \qquad (9.1)$$

The additional hydrogen ions released by carbonic acid bind to carbonate ions (CO_3^{2-}), forming additional HCO_3^-.

$$H^+ + CO_3^{2-} \rightarrow HCO_3^- \qquad (9.2)$$

This reduces the concentration of CO_3^{2-} (black curve in Fig. 9.13), making it harder for marine creatures to take up CO_3^{2-} to form the calcium carbonate needed to build their exoskeletons.

$$Ca^{2+} + CO_3^{2-} \rightarrow CaCO_3 \qquad (9.3)$$

The two main forms of calcium carbonate used by marine creatures are calcite and aragonite. Decreasing the amount of carbonate ions in the water makes it more difficult for both calcite users (phytoplankton, foraminifera and coccolithophore algae (Fig. 9.14)), and aragonite users (corals, shellfish, pteropods and heteropods).

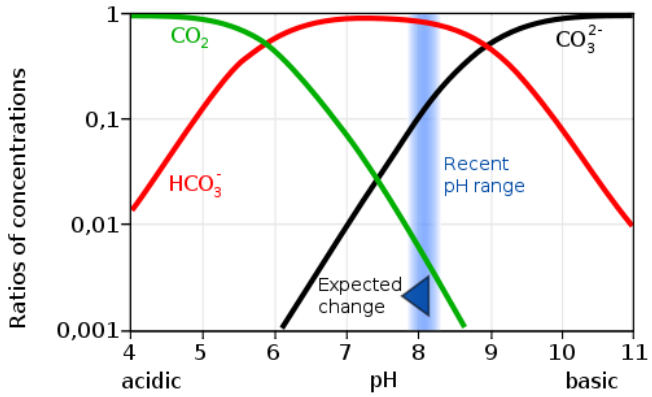

Figure 9.13. Ratios of the concentrations of CO_2, HCO_3^-, and CO_3^{2-} as a function of ambient pH. Typical present-day ocean values are shaded in blue.

Ocean acidification and species composition

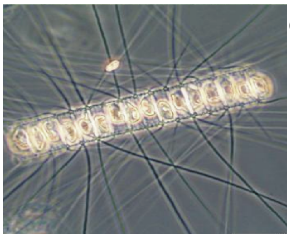

Chaetoceros costatus
(Diatom)

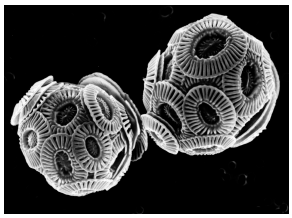

Emiliania huxleii
(Coccolithophorids)

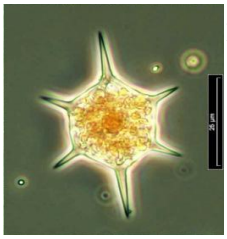

Distephanus speculum
(Silicoflagellate)

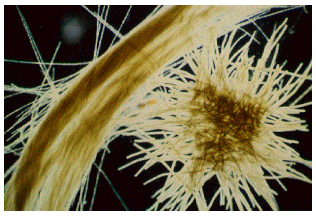

Trichodesmium
(Cyanobacterium)

Figure 9.14. Examples of oceanic species at the base of the food chain, including diatoms, coccolithophorids, silicoflagellates, and cyanobacteria.

Figure 9.15 shows that silicon-based life-forms live primarily at higher latitudes, while calcium carbonate life-forms dominate the food chain in the midlatitudes and the tropics. This implies that increased ocean acidification will have the strongest impact on the food chain in the midlatitudes and tropics.

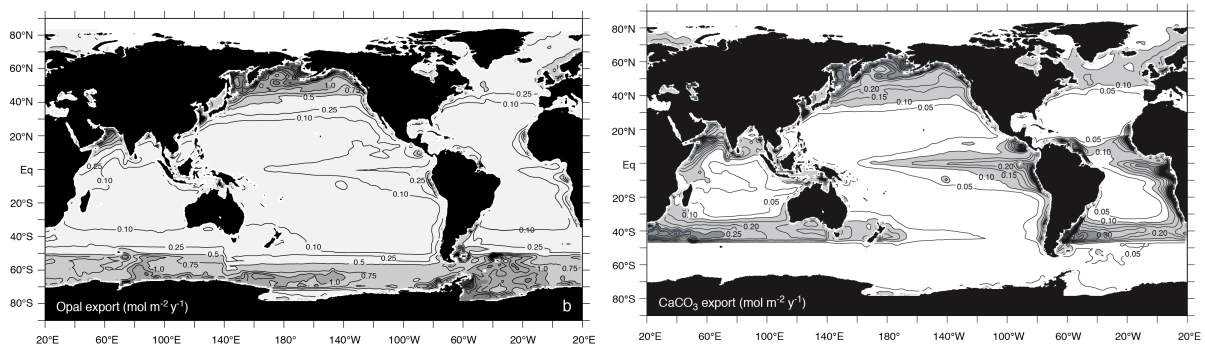

Figure 9.15. Annual distribution of the export of opal (silicate organisms) and $CaCO_3$ (coccolithophorids) from the upper layer of the ocean in mol m^{-2} yr^{-1} (Brasseur et al., 1999).

9.5. Recent trends in the methane budget

After carbon dioxide (CO_2), methane (CH_4) is the second most important greenhouse gas contributing to human-induced climate change. Methane is responsible for ~20% of the global warming produced by all greenhouse gases so far. The atmospheric life time of CH_4 is ~ 9 years. Methane contributes to the production of tropospheric ozone, which harms human

health and ecosystems. Methane also leads to the production of water vapor in the stratosphere by chemical reactions, enhancing global warming.

The evolution of atmospheric methane over the past two thousand years is shown in Fig. 9.16. Until ~1800 A.D., methane concentrations were ~700 ppbv. Over the past 200 years it has increased by a factor of ~2.5 to ~1800 ppbv, due to anthropogenic changes in land use.

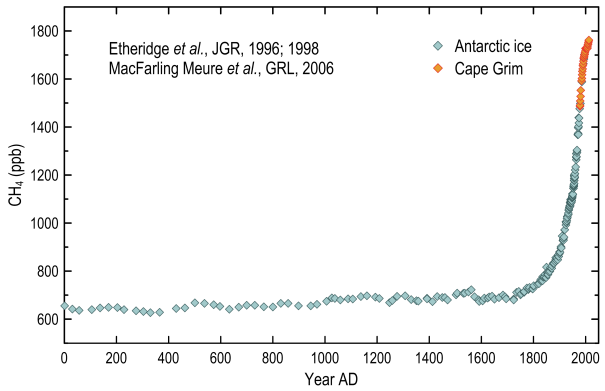

Figure 9.16. Evolution of methane concentration in the atmosphere over the past 2,000 years, as seen in Antarctic ice cores and atmospheric flask samples at Cape Grim, Tasmania.

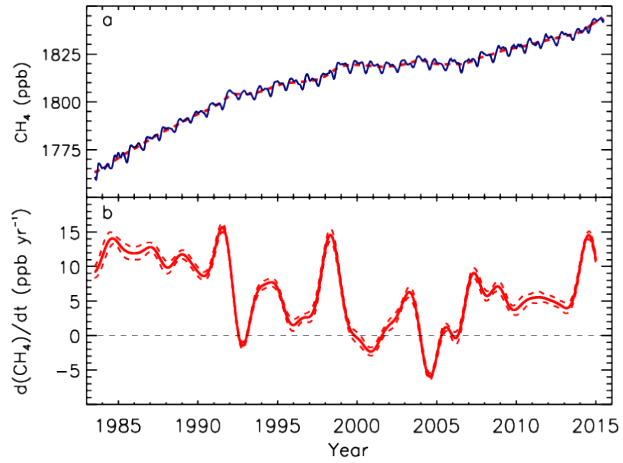

Figure 9.17. Evolution of a) methane concentration in the atmosphere (ppbv) and b) annual change in methane concentration (ppbv/yr) during 1984 – 2016.

The observed evolution of atmospheric methane concentration and its annual rate of change during 1984 – 2016 is shown in Fig. 9.17. There is an interesting reduction in the growth of atmospheric CH_4 concentrations during the early 2000s, which has been the subject of much speculation. After 2006, growth rates have been ~ 5-10 ppbv/yr, with concentrations reaching 1830 ppbv in 2015.

The geographical distribution of sources of methane from wetlands, fossil fuels, agriculture, biomass burning, and termites are shown in Fig. 9.18. Wetlands are the largest

natural global source of CH_4, being ~185 Tg CH_4/yr averaged for the period 2003-2012, with a range of 153–227 Gt CH_4/yr.

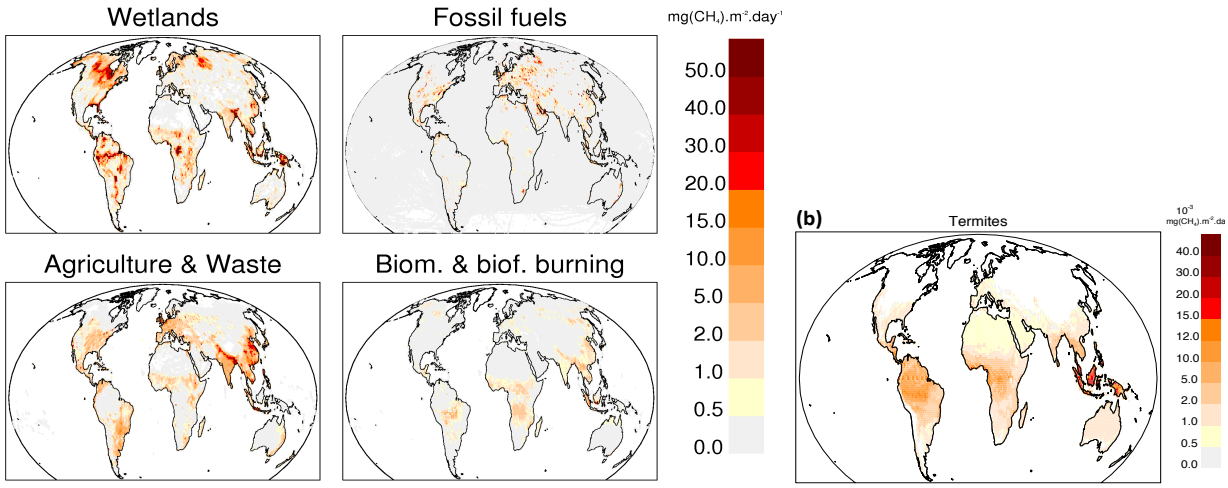

Fig. 9.18. a) Geographical distributions of methane sources from wetlands, fossil fuels, agriculture, biomass burning, and b) termites (mg CH_4 m^{-2} day^{-1}), based on carbon-cycle models constrained by observations (Fig. 3 of Saunois et al. 2016).

A global methane budget from the Global Carbon Project, averaged for the period 2003-2012, is shown in Fig. 9.19. All data are shown in Gt CH_4 for emissions and sinks, where an increase of 1 ppbv CH_4 corresponds to an increase of 2.78 Gt CH_4.

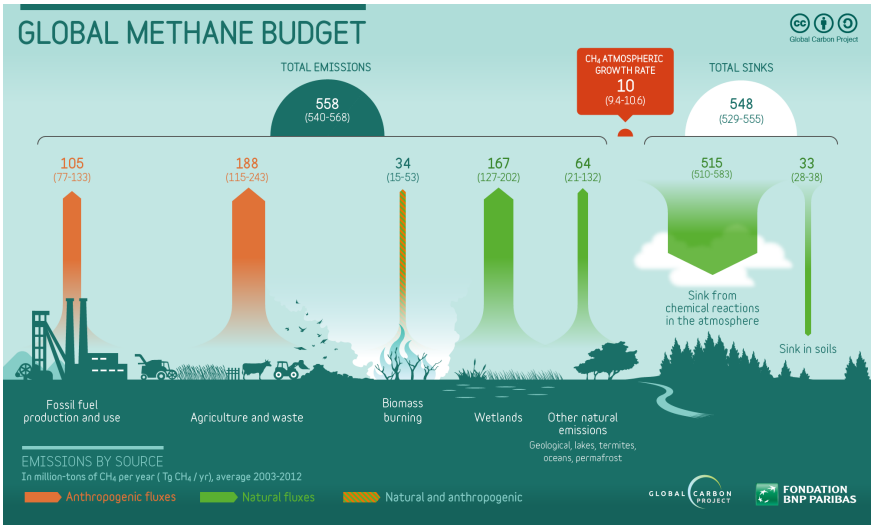

Figure 9.19. A global methane budget from the Global Carbon Atlas project, averaged for the period 2003-2012 (http://www.globalcarbonproject.org/methanebudget).

Total global emissions of methane are ~560 Tg CH_4/yr. The cause of the recent rise in global CH_4 concentrations is likely due to increased biogenic emissions, mostly from agriculture, and increased use of fossil fuels. Geographically, tropical regions play the most

significant role as contributors to the atmospheric growth. It is also possible that a decrease in scavenging by hydroxyl radicals has contributed to increases of methane in the last decade.

9.6. Future scenarios

The intergovernmental panel on climate change has issued a series of diagnoses and forecasts, based on the work and consensus of hundreds of scientists. The general approach to forecasting future climate is to run a suite of climate models into the future (an ensemble forecast), based on certain sets of economic assumptions. Figure 9.20, from Fuss et al. (2014) summarizes these forecasts out to 2100. At present, we are closest to the red trajectory (RCP8.5) regarding emission of CO_2. (Note that emission rates for CO_2 are 3.6 times that of carbon.) If the world's economic growth and fossil fuel usage follows this curve, by the year 2100 we will be emitting 100 Gt CO_2/yr (~30 Gt carbon/yr), or about 3 times as much as at present. This implies that atmospheric CO_2 concentration will likely exceed 1000 ppmv (~4x pre-industrial CO_2 loading) and that the globally averaged temperature will increase by ~3.2-5.4°C or ~6-10°F relative to the year 1900. If we are able to reduce the rate of fossil fuel use somewhat (RCP6), following the black curve, atmospheric CO_2 concentration will likely be in the range 700-1000 ppmv (~3x pre-industrial CO_2 loading) and that the globally averaged temperature will increase by ~2-3.7°C or ~4-7°F relative to the year 1900.

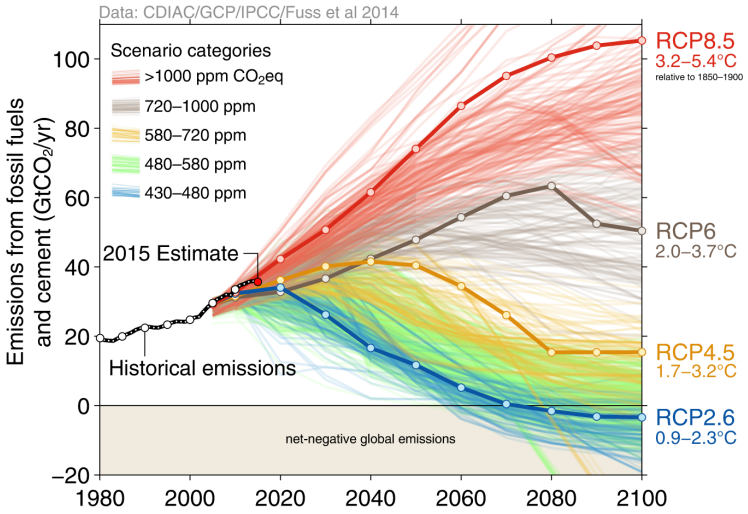

Figure 9.20. IPCC (2014) forecasts for the year 2100 of economic emission scenarios RCP8.5, RCP6, RCP4.5, and RCP2.6. The ensemble spread among models is shown in light lines for each scenario, with the average shown with a heavy line. Corresponding increases in atmospheric CO_2 concentration and range of global temperature increase are shown for each scenario.

The geographical distribution of the average model forecast temperature change in °C from IPCC (2009) for the decades 2020-2029 and 2090-2099 are shown in Fig 9.21 for scenarios B1 (upper), A1B (middle), and A2 (lower), similar to IPCC 2014 scenarios RCP4.5, 6, and 8.5. Note the markedly amplified forecast temperature increases in the high latitudes of

the NH. This approximate doubling of arctic temperature increases relative to global average is anticipated due to the ice albedo feedback. As the arctic warms, there will be less snow and ice to reflect sunlight, making the region even warmer.

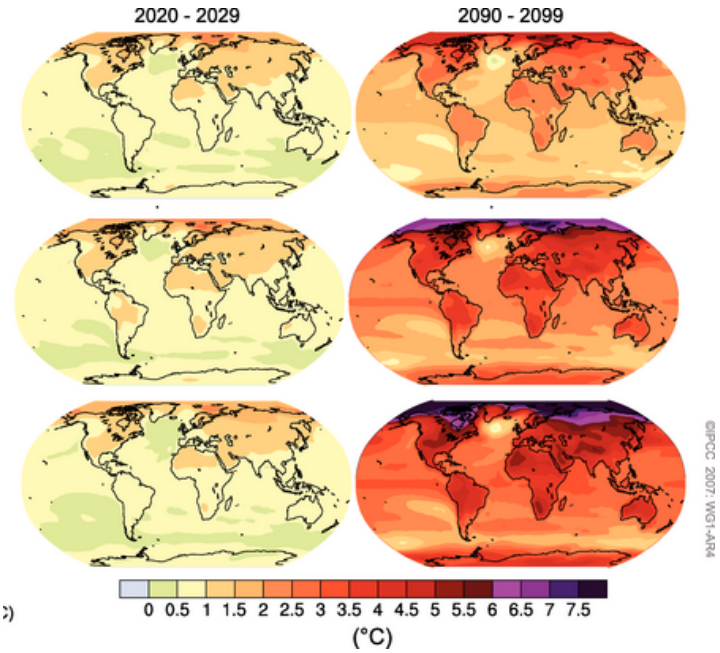

Figure 9.21. Geographical distribution of average model forecast temperature change in °C from IPCC (2009) for the decades 2020-2029 and 2090-2099 for scenarios B1 (upper), A1B (middle), and A2 (lower), similar to IPCC 2014 scenarios RCP4.5, 6, and 8.5.

The geographical distribution of average model forecast percent changes in precipitation for scenario A1B (similar to IPCC 2014 scenario RCP6) in 2100 is shown in Fig. 9.22. While models differ significantly, and precipitation is a notoriously difficult quantity to simulate accurately in current weather models, a consensus is apparent. The tropics and high latitudes are expected to have more precipitation, while the subtropics are forecast to have significantly less precipitation by the year 2100 A.D. If this were to come to pass, it would represent a serious challenge for adjusting where our global food supply can be successfully grown. To first order, Russia and Canada will be able to grow more food, but the populous subtropics will experience increasing difficulty in a drying climate.

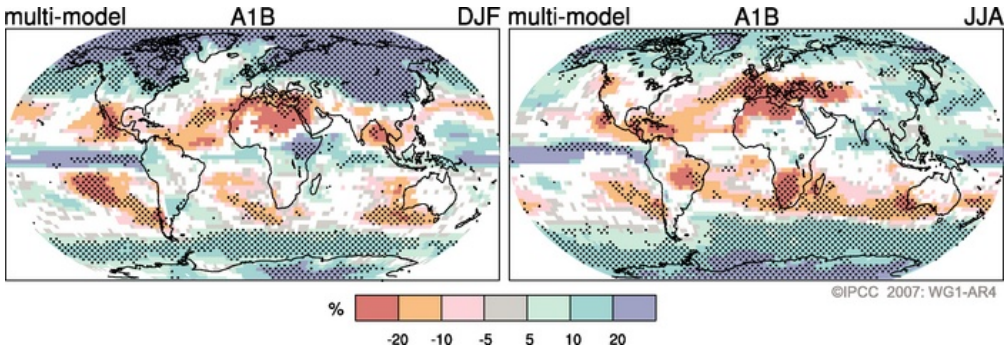

Figure 9.22. IPCC (2009) average model forecast for percent change in precipitation for scenario A1B (similar to IPCC 2014 scenario RCP6) in 2100.

One of the more interesting possibilities in future climate model forecasts is shown in Fig. 9.23. In coupled ocean-atmosphere models, with increasing atmospheric loadings of CO_2, a region of cooling is found in the high latitude North Atlantic basin. Due to the increase in high latitude precipitation and river runoff, freshening of the North Atlantic can make it more likely for sea ice to form during the winter, extending to lower latitudes relative to at present. This would have the effect of cutting off the heat flux from the ocean to the atmosphere, making the atmosphere colder. This would also reduce cooling of the upper ocean and therefore reduce the likelihood of sinking and forming bottom water, which would, in turn, reduce the sequestering of CO_2 in the deep North Atlantic. Under this scenario, Iceland and northwestern Europe may experience much harsher winters, even as the rest of the world warms considerably! This possibility is the basis for the movie "Day After Tomorrow", although the movie contains many meteorological errors.

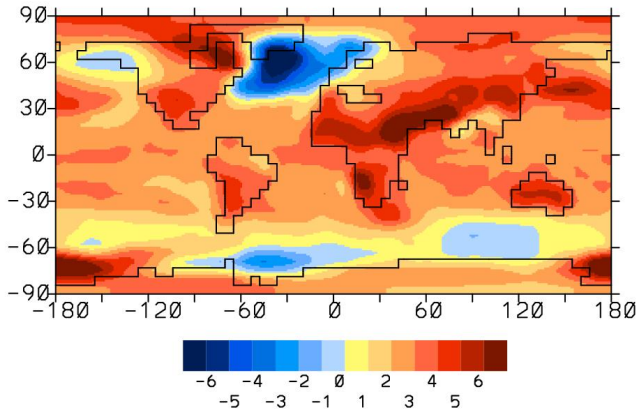

Figure 9.23. Distribution of forecast temperature change in °C for the year 2100 in a 4 x present CO_2 loading.

By the year 2100 we may have already started to access some of the gas hydrates that trapped in a frozen form beneath the sediments of the continental shelf. Figure 9.24 shows a pie chart of organic carbon in earth reservoirs, with methane clathrates being the largest category at 10,000 Gt carbon. If this methane were to be released to the atmosphere, it could augment global warming much more than shown RCP8.5 in Fig. 9.20.

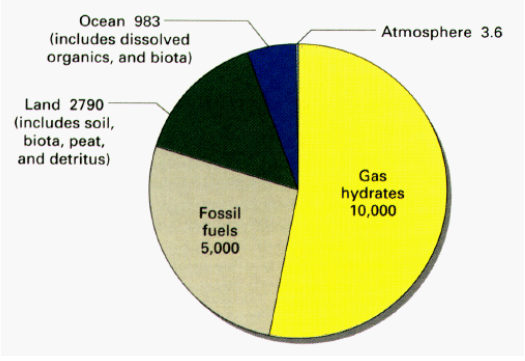

Figure 9.24. Estimated distribution of organic carbon (Gt C) in earth reservoirs.

References Cited

Brasseur, G. P., J. J. Orlando, and G. S. Tyndall, 1999: *Atmospheric Chemistry and Global Change,* Oxford University Press, New York, 654 pp.

Global Carbon Project Website https://www.globalcarbonproject.org/

Global Methane Budget Website http://www.globalcarbonproject.org/methanebudget

Suarez et al., 2019, *Oct. Elements*.

Saunois et al. 2016, ESSD

Recommended Movies of the Carbon Cycle

Carbon dioxide emissions from fossil fuels and cement production, from 1751 to 2007:
https://www.globalcarbonproject.org/carbonbudget/19/visualisations.htm

A year in the life of CO_2:
http://svs.gsfc.nasa.gov/goto?11719